INT. J. NUM. METH. HEAT FLUID FLOW, VOL. 2, 115–125 (1992)

THERMAL ANALYSIS OF SPACE TRUSSES INCLUDING THREE-DIMENSIONAL EFFECTS

OMRI RAND AND DAN GIVOLI

Department of Aerospace Engineering, Technion—Israel Institute of Technology, Haifa 32000, Israel

ABSTRACT

A numerical procedure is devised for the thermal analysis of three-dimensional large truss-type space structures exposed to solar radiation. Truss members made of an orthotropic material with a closed thin-walled cross-section of arbitrary shape are considered. Three-dimensional thermal effects are taken into account in the analysis. In the proposed method, the governing equations are first put into a weak form. Then the Galerkin finite element method is applied with respect to the axial coordinate of each truss member. The circumferential variation of the temperature is treated by a symbolically-coded harmonic balance procedure. The interaction between the various truss members is controlled by an iterative scheme. As a numerical example which demonstrates the proposed method, the temperature distribution in a parabolic dish structure is found. The results are compared to those obtained by standard one- and two-dimensional analyses.

KEY WORDS Space trusses 3-D thermal analysis

INTRODUCTION

The need for the thermal and thermoelastic analyses of large truss-type space structures, has grown significantly in the last few years. It has required special considerations not only in the application of numerical solution techniques but also in the mathematical modelling. The thermal problems involved are usually highly non-linear due to the presence of thermal radiation and non-linear material behaviour. In addition, the three-dimensional discretization of a large space structure would typically require a very large number of degrees of freedom if accurate results are desired. For this reason, in most of the previous works that dealt with the detailed thermal analysis of space structures, only one- or two-dimensional models were considered whereas three-dimensional effects were neglected.

The underlying assumption in a one-dimensional thermal analysis is that the temperature variation within the cross-section of any of the rods comprising the structure may be neglected in comparison with the variation along the axial direction of the rod. This assumption is justified for space structures composed of sufficiently slender rods and made of thermally high-conductive materials such as metals. If one proceeds to compute the elastic deformation and stresses generated by the temperature field thus derived, the structural response in terms of tension, compression and buckling of various truss members can be obtained.

Works that have adopted the one-dimensional approach include those of Thornton and his co-workers[1–3], Ko[4], and Givoli and Rand[5,6]. Thornton *et al.*[1] describe an integrated thermal–structural finite element formulation with solar radiation, and use a three member module of an orbiting truss as a testing model. Thornton and Paul[2] review the subject of computerized thermal–structural analysis of large space structures, and use for illustration a tetrahedral truss structure as a model for a microwave radiometer system. Mahaney and

0961–5539/92/020115–11$2.00

Received April 1991
Revised October 1991

Thornton[3] investigate the effects of self-shadowing on the thermal–structural behaviour of space structures. Ko[4] describes in detail the thermal and elastic analyses performed for the space shuttle orbiter, including internal convection and radiation effects. Givoli and Rand[5,6] propose a numerical method for thermal and elastic problems with periodic loading, which combines finite element spatial discretization in the axial direction and spectral treatment in time.

A different approach is based on a two-dimensional analysis, and in a sense is complementary to the previous analysis. This approach starts from the assumption that the temperature variation along the axial direction of each rod is negligible with respect to the variation through the cross-section. This assumption has been shown to be appropriate for structures with slender thin-walled members made of laminated composite materials such as graphite/epoxy[7]. This type of response in a fibre/matrix material originates from the low thermal conductivity of the material in the axial direction. The temperature variation through the cross-sections of the structural members produces in turn elastic bending. The corresponding displacements and stresses can be obtained by performing a structural analysis on the basis of the results from the thermal analysis.

The two-dimensional approach was adopted in the works by Mahaney *et al.*[8] and Lutz *et al.*[9]. In the latter paper, the authors propose to use different finite element models for the thermal and structural analyses of a frame-type structure. The temperature field is first determined at selected cross-sections of some of the beam members, via a two-dimensional finite element thermal analysis. The forces and moments due to this temperature distribution are then calculated, and the global structural response of the structure is obtained from the elastic finite element model of the entire frame.

The present paper proposes a numerical procedure for the three-dimensional thermal analysis of truss-type space structures. This means that both the axial and cross-sectional variations of the temperature are taken into account. The proposed procedure makes an effective tool for the analysis of both metallic and composite space structures with either long or short members. It can also be used as a first step in a detailed three-dimensional thermoelastic analysis.

A straightforward use of a standard numerical method, such as the finite element method, for the solution of the governing equations in the three-dimensional domain defined by the structure, typically requires a very large computational effort, due to the tremendous number of degrees of freedom involved (see e.g. Chin *et al.*[10]). To avoid this aspect of the analysis, a special procedure is adopted in this paper. First, the governing equations are put into a weak form. Then a Galerkin finite element discretization is applied, but only with respect to the *axial coordinate* of each truss member separately. This results in a non-standard finite element formulation. The *circumferential variation* of the temperature is decomposed spectrally, and the Fourier coefficients of this decomposition are found by a symbolically-coded harmonic balance procedure developed in Rand and Givoli[11]. Finally, the interaction between the various truss members is controlled by an iterative scheme. Thus, the finite element spectral procedure outlined above is repeated in each iteration.

In a numerical example which demonstrates the proposed method, we find the temperature distribution in a parabolic antenna dish exposed to solar radiation. We examine the influence of the dish orientation with respect to the radiation vector on the thermal response. Also, the results from the three-dimensional analysis are compared to those obtained by the corresponding one- and two-dimensional models.

FINITE ELEMENT FORMULATION

Consider a composite truss-type structure where each truss member has a uniform thin-walled closed cross-section of an arbitrary shape. *Figure 1* shows a typical member in the structure. The axial coordinate is denoted ξ, and the circumferential coordinate along the midline of the thin cross-section is denoted s. The latter coordinate starts from an arbitrary point on the midline and measures arclength along this line. The maximum value of s, namely the

cross-sectional perimeter, is denoted p. The member's length is L and the thickness of the cross-section is t. The exterior surface of the rod is exposed to solar radiation.

Some simplifying assumptions are made in the present model. The edges $\xi=0$ and $\xi=L$ are assumed to converge geometrically to fit into the joints which connect the rod to other structural members. In these edges the cross-section is characterized by a single temperature, assumed to be identical for all the rods connected to the same joint. In other words, the joints are considered perfect conductors and lacking any heat capacity. In addition, it is assumed that two usually weak effects can be neglected, namely heat exchange through radiation between different truss members, and the thermodynamic influence of the elastic strain rate on the temperature field.

The equation of steady-state heat conduction and radiation which holds in the three-dimensional domain defined by the rod is:

$$\nabla\cdot(\kappa\nabla u)-C_R u^4+q=0 \tag{1}$$

Here $u(\xi,s)$ is the temperature, $\kappa=[\kappa_{ij}]$ is the thermal conductivity tensor for the anisotropic material under consideration, C_R is the radiation coefficient, and q is the given solar incident flux. The coefficient C_R is given by:

$$C_R=\frac{\sigma\varepsilon}{t} \tag{2}$$

where σ is the universal Stefan–Boltzmann constant, and ε is the surface emissivity of the member. The incident flux q is calculated by:

$$q(s)=\frac{\alpha\beta_0\beta_s(s)}{t}q_{\text{sun}} \tag{3}$$

Here q_{sun} is the absolute value of the solar radiation vector, α is the surface absorptivity, β_0 is the 'view factor' associated with the orientation of the rod with respect to the solar radiation vector, and $\beta_s(s)$ is the 'view factor' depending on the direction of the normal $\mathbf{n}$ to the outer surface of the cross-section at each point on the surface (see *Figure 1*). Both 'view factors' can have values between zero and one.

The inclusion of the radiation and the heat flux terms in the differential equation (1) (rather than in the boundary conditions) and the presence of the factor $1/t$ in (2) and (3), originate from the fact that the rod is thin-walled and thus temperature variation through the cross-section in the direction normal to s is negligible. Equation (1) is supplemented by two boundary conditions at the edges $\xi=0$ and $\xi=L$ and also by the requirement that the temperature $u(\xi,s)$ is a periodic function in s with period p. The two boundary conditions at the edges are Dirichlet conditions, namely:

$$u(0,s)=T_1 \qquad u(L,s)=T_2 \tag{4}$$

where T_1 and T_2 are regarded, for the time being, as given temperatures.

For simplicity, it is further assumed that the conductivity tensor κ in (1) has its principal directions along the ξ and s axes. In other words, the composite fibre matrix configuration of the rod is such that each rod is associated with two effective conductivities: the axial conductivity κ_ξ and the circumferential conductivity κ_s. Also, it should be noted that for thin-walled members the exact shape of the cross-section is irrelevant as far as heat conduction is concerned; the detailed cross-sectional geometry is important only for the determination of the radiation view factor β_s in (3). In this light, the first term in (1) becomes:

$$\nabla\cdot(\kappa\nabla u)\equiv\frac{\partial}{\partial\xi}\left(\kappa_\xi\frac{\partial u}{\partial\xi}\right)+\frac{\partial}{\partial s}\left(\kappa_s\frac{\partial u}{\partial s}\right) \tag{5}$$

Now the Galerkin finite element is applied to (1) and (4) *with respect to ξ only*. Thus, each rod is divided into one-dimensional finite elements in the ξ direction, whereas variation with

respect to the variable s remains continuous. This results in the following system of ordinary differential equations in the variable s:

$$\mathbf{M}\mathbf{d}_{ss}(s)+\mathbf{K}\mathbf{d}(s)+\mathbf{R}(\mathbf{d}(s))=\mathbf{F}(s) \tag{6}$$

where

$$\mathbf{M}=A_{e=1}^{N_{el}}\mathbf{m}^e \qquad \mathbf{K}=A_{e=1}^{N_{el}}\mathbf{k}^e \qquad \mathbf{R}=A_{e=1}^{N_{el}}\mathbf{r}^e \qquad \mathbf{F}=A_{e=1}^{N_{el}}\mathbf{f}^e$$
$$\mathbf{m}^e=[m_{ab}^e] \qquad \mathbf{k}^e=[k_{ab}^e] \qquad \mathbf{r}^e=\{r_a^e\} \qquad \mathbf{f}^e=\{f_a^e\} \tag{7}$$

Here N_{el} is the total number of elements in the rod in the ξ direction, $A_{e=1}^{N_{el}}$ is the assembly operator, and $\mathbf{m}^e$, $\mathbf{k}^e$, $\mathbf{r}^e$ and $\mathbf{f}^e$ are the element matrices and vectors corresponding to the global matrices and vectors **M**, **K**, **R** and **F**. The subscript ss in (6) stands for the second derivative with respect to s. In (6), **d** is the global solution vector containing the nodal temperatures, and **R** is the radiation vector which depends non-linearly on **d** (see (10) below). The expressions for the element matrices and vectors are:

$$m_{ab}^e=-\int_{\Omega^e} N_a\kappa_s N_b\,\mathrm{d}\xi \tag{8}$$

$$k_{ab}^e=\int_{\Omega^e} N_a'\kappa_\xi N_b'\,\mathrm{d}\xi \tag{9}$$

$$r_a^e=\int_{\Omega^e} N_a C_R\left(\sum_{b=1}^{N_{en}} T_b(t)N_b(s)\right)^4\mathrm{d}\xi \tag{10}$$

$$f_a^e=\int_{\Omega^e} N_a q\,\mathrm{d}\xi-\sum_{b=1}^{N_{en}} T_b^e k_{ab} \tag{11}$$

Here Ω^e is the element domain, N_a is the element shape function associated with node a, N_{en} is the number of element nodes, and

$$T_b^e=\begin{cases} T_1 & \text{if } e=1 \text{ and } b=1 \\ T_2 & \text{if } e=N_{el} \text{ and } b=N_{en} \\ 0 & \text{otherwise} \end{cases} \tag{12}$$

The prime in (9) indicates differentiation with respect to ξ.

The finite element matrix formulation (6)–(12) is clearly non-standard is some aspects, although it has a remarkable resemblance to the standard semi-discrete formulation in the one-dimensional time-dependent case, where s is analogous to time (see e.g. Hughes[12]). The matrix $\mathbf{m}^e$ is similar to the so-called element heat capacity matrix, with two differences: there is a minus sign in front of the integral in (8), and the coefficient appearing in the integrand is the conductivity κ_s rather than the heat capacity. Moreover, in (6) the matrix **M** multiplies the *second* s-derivative of the solution vector **d**. In this respect the formulation is more similar to that of structural dynamics, where $\mathbf{m}^e$ is analogous to the element mass matrix. However, the expressions (9)–(11) for the conductivity matrix $\mathbf{k}^e$, the radiation vector $\mathbf{r}^e$ and the thermal load vector $\mathbf{f}^e$ are standard.

Explicit expressions for (8)–(11) for a specific choice of shape functions can easily be obtained. In fact, such expressions are analogous to those corresponding to the one-dimensional time-dependent case[11,12], except that the standard expression for $\mathbf{m}^e$ has to be modified according to the remarks made previously. For example, in the case where $N_{en}=2$ and $N_a\,(a=1,2)$ are the linear shape functions, and assuming that κ_s has the constant value κ_s^e in element e, (8) gives:

$$\mathbf{m}^e=-\frac{\kappa_s^e h^e}{6}\begin{bmatrix}2 & 1\\ 1 & 2\end{bmatrix} \tag{13}$$

where h^e is the element length.

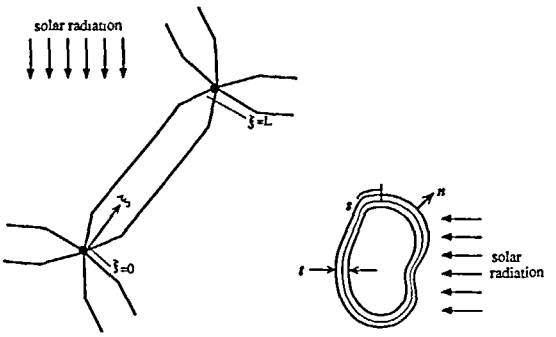

Figure 1 Typical member in a space structure

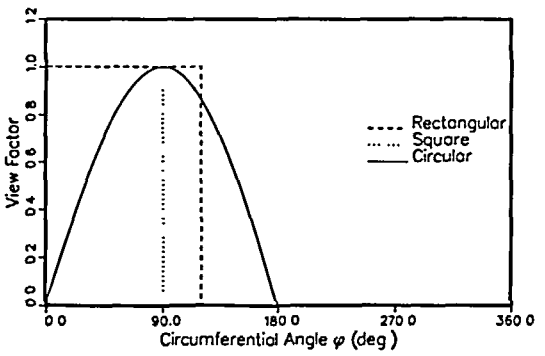

Fig. 2b

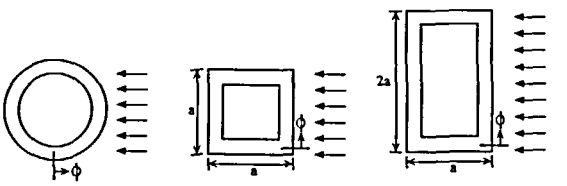

Fig. 2a

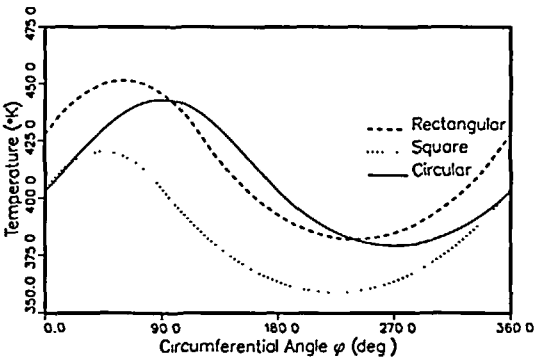

Fig. 2c

Figure 2 Effect of the shape of the cross-section on the thermal behaviour. (a) Geometry of three thin-walled cross-sections. (b) Corresponding view factors β_s. (c) Temperature distribution along the perimeter of the three cross-sections

ANALYSIS IN THE CIRCUMFERENTIAL DIRECTION

The solution of the system of ordinary differential equations (6) has to be considered next. The method of solution of this system is based on the spectral method devised by Rand and Givoli[11] in the time-periodic one-dimensional context. In this method, each s-dependent function in (6) is decomposed, using the discrete Fourier transform, into a finite number of harmonics, N, and the Fourier coefficients are found using a non-linear harmonic balance analysis. The idea to combine a finite element scheme with harmonic balance analysis was also recently proposed by Lewandowski[13] for vibrating structures.

To be more specific, consider any vector $\mathbf{g}(s)$ appearing in (6). This vector is approximately represented by the finite Fourier expansion,

$$\mathbf{g}(s) \simeq \mathbf{g}_0 + \sum_{n=1}^{N} (\mathbf{g}_{cn} \cos n\phi + \mathbf{g}_{sn} \sin n\phi) \tag{14}$$

Here $\mathbf{g}_0$, $\mathbf{g}_{cn}$ and $\mathbf{g}_{sn}$ $(n=1,\ldots,N)$ are real constant vectors, and ϕ is the circumferential angle defined by $\phi = 2\pi s/p$. Denoting the right hand side of (14) by the 'harmonic operator' $\mathscr{H}_N(\mathbf{g}_0, \{\mathbf{g}_{cn}\}, \{\mathbf{g}_{sn}\})$, we can write (14) as:

$$\mathbf{g} \simeq \mathscr{H}_N(\mathbf{g}_0, \{\mathbf{g}_{cn}\}, \{\mathbf{g}_{sn}\}) \tag{15}$$

Now, basic arithmetic operations can be performed with the harmonic representation (15). For example, given the two functions $f \simeq \mathscr{H}_N(f_0, \{f_{cn}\}, \{f_{sn}\})$ and $g \simeq \mathscr{H}_N(g_0, \{g_{cn}\}, \{g_{sn}\})$ and the

real constants a and b, it is easy to see that:

$$\frac{\partial^j f}{\partial \phi^j} \simeq (-1)^{(j+1)/2} \mathscr{H}_N(0, \{-n^j f_{sn}\}, \{n^j f_{cn}\}) \qquad j=1,3,5,\ldots \tag{16}$$

$$\frac{\partial^j f}{\partial \phi^j} \simeq (-1)^{j/2} \mathscr{H}_N(0, \{n^j f_{cn}\}, \{n^j f_{sn}\}) \qquad j=2,4,6,\ldots \tag{17}$$

$$af + bg \simeq \mathscr{H}_N(af_0 + bg_0, a\{f_{cn}\} + b\{g_{cn}\}, a\{f_{sn}\} + b\{g_{sn}\}) \tag{18}$$

The product fg can also be computed, and the result can be written in the form:

$$fg \simeq \mathscr{H}_N(h_0, \{h_{cn}\}, \{h_{sn}\}) \tag{19}$$

Expressions for the Fourier coefficients of the product, h_o, $\{h_{cn}\}$ and $\{h_{sn}\}$, are given in Reference 11.

All the variables in (6), namely all the entries of the vectors **d**, **R** and **F**, are expanded via (15). The Fourier coefficients $\mathbf{F}_0$, $\mathbf{F}_{cn}$ and $\mathbf{F}_{sn}$ associated with the thermal load vector **F** are found using a fast Fourier transform (FFT) scheme. The decomposition of the radiation vector **R** into its Fourier components is more involved and is considered now. First, we note that the kth entry of this vector, R^k, has the general form:

$$R^k(\mathbf{d}) = \sum_{l=1}^{N_{cn}} \sum_{j=0}^{4} A_{jkl} (d^k)^j (d^l)^{4-j} \tag{20}$$

Here d^k is the kth entry of the vector **d**, and the A_{jkl} are constants, where $A_{jkl} \neq 0$ only if node k and node l belong to the same element. The form (20) follows from the expression (10) for the element radiation vector, from the additive character of the assembly operator in (7), and from the property of locality that finite elements possess. Now each term in (20) is a product of temperature variables. For example, if $j=3$ then

$$A_{jkl}(d^k)^j (d^l)^{4-j} = A_{3kl}(d^k)(d^k)(d^k)(d^l) \tag{21}$$

Thus, one can use the product formula (19) to compute R^k. All the calculations of this sort have been done symbolically by the computer code itself. We have used a symbolic manipulation program[14] which is particularly suitable for harmonic-type calculations.

After the Fourier expansions of **d**, **R** and **F** are substituted in (6), one obtains a non-linear coupled system of algebraic equations for the unknown coefficient vectors $\mathbf{d}_0$, $\mathbf{d}_{cn}$ and $\mathbf{d}_{sn}$. Again, the formation of all these algebraic equations is performed symbolically by the code. The algebraic system of equations thus obtained is solved via a modified Newton–Raphson iterative procedure[11].

It should be noted that a standard 'time-integration' scheme can also be employed to solve the system (6), using finite differences in the variable s. However, in Reference 11 the comparison between the proposed spectral method and a standard time-integration is discussed, and the former is shown to be superior in many cases for solutions periodic in s.

ITERATIVE SCHEME FOR UPDATING JOINT TEMPERATURES

In the solution procedure outlined above for the temperature variation in the ξ and s directions it was assumed that all the joint temperatures were given, These joint temperatures were used in the boundary conditions (4) prescribed at the edges of each rod and appeared in the finite element formulation in (11) and (12). However, the joint temperatures are in fact unknown, and therefore an iterative scheme is needed to update them. The scheme starts from an 'initial guess' for all joint temperatures. Based on the these data, the finite element spectral analysis is performed for each rod separately, and the temperature field in the entire structure is found. Next all the joint temperatures are updated, according to the guidelines given below, and the finite element

spectral procedure is repeated. This yields a better solution, on the basis of which the joint temperatures are updated again, and so on. This process stops when convergence is achieved, namely when the differences between joint tempratures obtained in two successive iterations are sufficiently small.

The scheme adopted here for updating the joint temperatures is as follows. Consider a certain joint which connects together J rods. It is clear that the net amount of heat flux entering the joint from all J rods must be zero. This can be stated by:

$$\sum_{j=1}^{J} \int_{A_j} \kappa_\xi \frac{\partial u^*}{\partial \xi} \mathrm{d}A_j = 0 \tag{22}$$

where A_j is the cross-sectional area of rod j, and u^* is the approximate solution near the joint obtained by the finite-element spectral method. Now for the thin closed cross-section considered here we have $\mathrm{d}A_j = (t_j p_j / 2\pi)\mathrm{d}\phi$, where t_j and p_j are respectively the thickness and perimeter of rod j. Also, we replace $\partial u^*/\partial \xi$ by the finite difference approximation $(u^*|_{\xi=\Delta_j} - U)/\Delta_j$. Here Δ_j is the length of the first finite element belonging to rod j and starting from the joint, and U is the value of the temperature at the joint, which is common to all the rods $j = 1, \ldots, J$. This finite difference expression is in fact exact for linear two-node finite elements. Finally, we assume that κ_ξ in rod j has the constant value $\kappa_{\xi j}$ in the first element near the joint. Thus, (22) becomes:

$$\sum_{j=1}^{J} \frac{t_j p_j \kappa_{\xi j}}{2\pi\Delta_j} \int_0^{2\pi} (u^*|_{\xi=\Delta_j} - U)\,\mathrm{d}\phi = 0 \tag{23}$$

Now recall that $u^*(\xi, \phi)$ is composed of N ϕ-harmonics as in (14), i.e.:

$$u^* = u_0^* + \sum_{n=1}^{N} (u_{cn}^* \cos n\phi + u_{sn}^* \sin n\phi) \tag{24}$$

Only the zeroth-order harmonic u_0^* will contribute to the integral in (23), the average of all higher harmonics being zero. Thus (23) gives:

$$\sum_{j=1}^{J} \frac{t_j p_j \kappa_{\xi j}}{\Delta_j} (u_0^*|_{\xi=\Delta_j} - U) = 0 \tag{25}$$

Equation (25) can be solved for the joint temperature U, i.e.

$$U = \frac{\sum_{j=1}^{J} (t_j p_j \kappa_{\xi j}/\Delta_j) u_0^*|_{\xi=\Delta_j}}{\sum_{j=1}^{J} t_j p_j \kappa_{\xi j}/\Delta_j} \tag{26}$$

This formula holds for every joint separately. Thus, (26) is used for updating all the joint temperatures on the basis of the results obtained from the preceding finite element spectral analysis.

In the simplest case, when t_j, p_j, $\kappa_{\xi j}$ and Δ_j are *equal* for all the rods $j = 1, \ldots, J$, (26) reduces to:

$$U = \frac{1}{J} \sum_{j=1}^{J} u_0^*|_{\xi=\Delta_j} \tag{27}$$

In other words, the joint temperature U is simply the average of the temperature at the second node of all the rods connected to the joint.

Various numerical experiments show that the iterative procedure outlined above which incorporates the updating formula (26) converges rapidly if the initial guess for the joint temperatures is reasonably close to the exact solution there. However, when the initial guess was significantly different from the exact solution the process diverged in some cases. We have found that this divergence can be prevented by limiting the allowed change per iteration for each joint temperature. Thus, when (26) results in an update in U which is larger (in percentage)

than a specified value ΔU, then U is updated only with the amount ΔU. This modification leads to convergence in all the cases that we have tested, even when the initial guess was far from the exact solution.

CROSS-SECTIONAL GEOMETRY AND VIEW FACTORS

Two view factors, β_0 and $\beta_s(s)$, appear in (3) for the incident heat flux $q(s)$ on each truss member. The value of the view factor β_0 is determined from the orientation of the rod with respect to the solar radiation vector, and from information related to self-shadowing. We presented[5] an algorithm for the calculation of this view factor for general transparent/opaque rotating structures. The view factor $\beta_s(s)$ is calculated at each desired point on the perimeter of the cross-section from information associated to the geometrical shape of the cross-section.

Consider for example the three cross-sections depicted in *Figure 2a*. The direction of the solar radiation vector is also indicated in the Figure in each case. The view factors β_s corresponding to the three cases are shown in *Figure 2b*, as functions of the circumferential angle $\phi = 2\pi s/p$. The graph of β_s for the circular cross-section is that of a truncated sine function, the reason for the truncation being that one part of the cross-section overshadows the other part. For the same reason, the graph of β_s for the square and rectangular cross-sections has a step-function character.

We wish to demonstrate the influence that the shape of the cross-section has (through the view factor β_s) on the distribution of the temperature field. To this end we consider three infinite rods having the cross-sections shown in *Figure 2a*. The parameters are $\alpha = 0.92$, $\beta_0 = 1$, $t = 0.015$ m, $q_{\text{sun}} = 1300\,\text{W/m}^2$, $\kappa_\xi = k_s = 10.1\,\text{W/m K}$, and $C_R = 9.1 \times 10^{-7}\,\text{W/m}^3\,\text{K}^4$. We perform the spectral analysis to find the temperature in each case, bypassing the finite element and iterative procedures which are not needed in the case of an infinite rod. In *Figure 2c* the temperature distribution along the perimeter of the three cross-sections is shown. We see that although the view factors β_s for the three cross-sections, and subsequently the corresponding incident heat fluxes, are quite different from each other, the temperature distribution varies only slightly; there is a strong 'smoothing' effect on the temperature field. The maximum temperatures for the circle, square and rectangle are 438 K, 418 K and 450 K, respectively.

In the example above we have used 12 harmonics in the Fourier expansions of all the variables, namely we chose $N = 12$ in the representation (14). Although the first harmonic was dominant, as suggested from *Figure 2c*, it is not true that a much smaller number of harmonics than 12 would yield results with the same numerical accuracy. Owing to the non-linear character of the analysis, the contribution of the coupling between two higher-order harmonics, say the third and fourth harmonics, to the first harmonic may be important even if the amplitudes of these two harmonics are relatively small. Notwithstanding, to obtain the results shown in *Figure 2c*, the circular cross-section required a slightly smaller number of harmonics than did the rectangular and square cross-sections.

In general, one must make an adequate choice of the number of harmonics N in order to obtain accurate results. This can be done by performing a convergence test; if the addition of a few harmonics has only a minor effect on the results, then the number of harmonics is probably sufficient. In addition, if the last few harmonics of the results are not negligible with respect to the first harmonics then N must be increased. By using these two criteria one is able to find the necessary number of harmonics in a specific problem.

TEMPERATURE DISTRIBUTION IN AN ANTENNA DISH

Consider the graphite–epoxy parabolic dish structure shown in *Figure 3*. Such a dish can be used either as a concentrator for solar radiation or as an antenna for communication. The thermal and geometrical data are the same as in the previous section, except that here $\alpha = 0.28$. The radii of the inner and outer rings are 5 and 20 m, respectively, and the depth between these rings is 6 m. The global cartesian coordinate system x–y–z is introduced as shown in *Figure 3*.

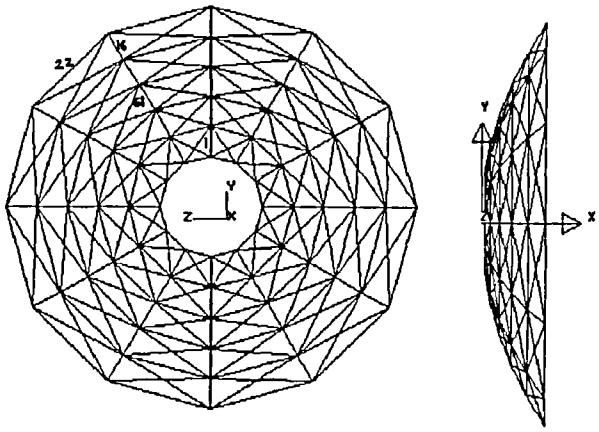

Figure 3 Parabolic antenna dish model

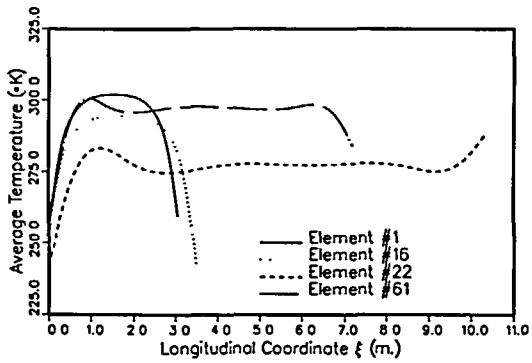

Figure 4 Three-dimensional analysis: average cross-sectional temperatures along the axes of rods 1, 16, 22 and 61, at orientation angle $\psi = 90°$

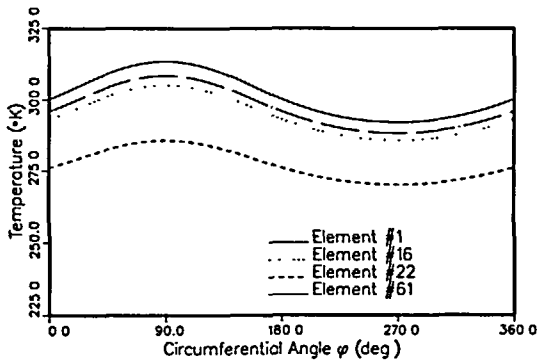

Figure 5 Three-dimensional analysis: mid-rod temperature along the cross-sectional perimeter of rods 1, 16, 22 and 61, at orientation angle $\psi = 90°$

All the truss members have a thin circular cross-section of radius 0.1 m. Each member in the structure is divided into *seven* finite elements with *linear* shape functions. These elements are not equally spaced, but rather graded using a cosine distribution in which the density of the elements is larger near the two edges than in the middle of the rod. In *Figure 3* the rods numbered 1, 16, 22 and 61 are indicated for future reference. Again we use 12 harmonics in the Fourier expansions of all the variables.

Suppose the solar radiation vector lies in parallel to the x–z plane, and forms an angle ψ with the negative-x axis. The dish is assumed to have a constant orientation with respect to the radiation vector, or else its orientation is assumed to change in time sufficiently slowly so that the response can be considered quasi-steady. (See Givoli and Rand[5] for a discussion on the conditions permitting this assumption.)

First, we use the procedure proposed previously to obtain the three-dimensional distribution of temperatures in the structure, with $\psi = 90°$. In this case, the solar radiation vector is pointing in the $-z$ direction. Based on the results of this analysis, *Figure 4* shows the average temperature in the cross-section (u_0^* in (24)) as a function of the axial coordinate ξ for rods 1, 16, 22 and 61. *Figure 5* shows the temperature distribution around the cross-section for the middle sections ($\xi = L/2$) of rods 1, 16, 22 and 61. The results demonstrate that the position of the rod in the

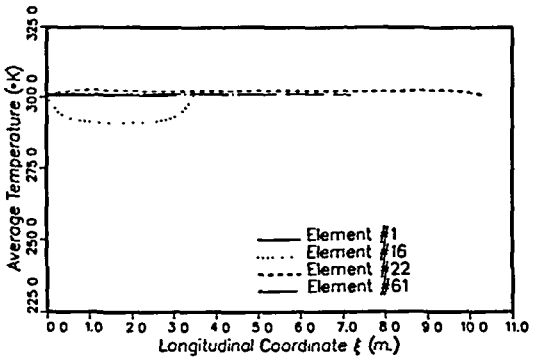

Figure 6 Three-dimensional analysis: average cross-sectional temperatures along the axes of rods 1, 16, 22 and 61, at orientation angle $\psi = 0°$

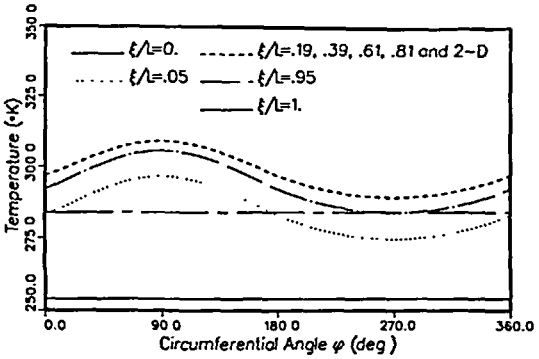

Figure 7 Comparison of the temperature distribution along the perimeter of rod 61 as obtained by the two-dimensional analysis with the temperature distribution at eight axial locations as obtained by the three-dimensional analysis

structure and its orientation have a significant influence on the temperature distribution both in the axial direction and in the circumferential direction.

Now we repeat the three-dimensional analysis for $\psi = 0°$. In this case the solar radiation vector is pointing in the $-x$ direction, namely in the direction of the dish axis. *Figure 6* shows the average temperature in the cross-section as a function of ξ. Comparing this Figure to *Figure 4* we see that the temperature distribution is much more uniform in the $\psi = 0°$ case than in the $\psi = 90°$ one. Moreover, all the rods except rod 16 have the same average temperature, namely about 300 K.

Next, we set the orientation angle again to be $\psi = 90°$, and we compare the results obtained above to those which may be obtained by simpler one- and two-dimensional analyses. The one-dimensional approach ignores temperature distribution through the cross-section. The results for the temperature as a function of the axial coordinate ξ for rods 1, 16, 22 and 61 obtained from a one-dimensional analysis turn out to coincide with those for the three-dimensional *average* temperature shown in *Figure 4*. This is, in fact, expected since the one-dimensional model is supposed to describe the average behaviour in the cross-section of the three-dimensional model. However, the one-dimensional approach does not provide any information on the cross-sectional temperature variation. Consequently, no information is available with regard to the elastic bending of the various rods as a result of the thermal loading.

Finally, we consider the two-dimensional approach, which assumes uniformity of the temperature field in the rod axial direction. In *Figure 7* the temperature around the cross-section (at any location) of rod 61 obtained by the two-dimensional analysis, is compared to the temperature distribution obtained by the three-dimensional analysis around the cross-sections at eight locations of rod 61. These eight locations on the axis of the rod are the locations of the finite element nodal points. It is apparent from *Figure 7* that the two-dimensional distribution coincides with the three-dimensional distribution at nodes 3–6 (in the central region of the rod), but that at the other four locations the results of the two analyses differ significantly. Moreover, in the two-dimensional approach information regarding the variation of temperatures or thermal stresses in the axial direction is unavailable.

CONCLUSION

In this paper we have proposed a special numerical procedure for the solution of thermal problems of truss-type space structures, which takes into account three-dimensional effects. The analysis based on this procedure produces the temperature distribution along the truss members

as well as through the cross-section. The proposed method avoids the need for a large number of degrees of freedom which is typical when using the standard finite element and finite difference methods in three dimensions. It was shown that in some situations one- and two-dimensional analyses do not provide sufficient or accurate information on the temperature distribution, and a three-dimensional analysis is required. Another important advantage of the proposed method is that it can serve as a first step in producing detailed three-dimensional thermoelastic information.

Future investigation will include the extension of the proposed method to more complicated situations, e.g. problems involving rotating structures, thermal-elastic coupling, material non-linearity, and exchange of radiation among different members. In addition, an elastic analysis based on the results of the thermal analysis will be performed, and conclusions with regard to some optimal thermoelastic parameters of the structure will be drawn.

ACKNOWLEDGEMENT

This work was supported in part by the L. Kraus Research Fund, V.P.R. Fund no. 160–643, and by the Adler Fund for Space Research.

REFERENCES

1 Thornton, E. A., Dechaumphai, P. and Wieting, A. R. Integrated finite element thermal-structural analysis with radiation heat transfer, *23rd Structures, Struct. Dyn. Mat. Conf.* (Part 1), AIAA Publication, pp. 188–196 (1982)
2 Thornton, E. A. and Paul, D. B. Thermal–structural analysis of large space structures: an assessment of recent advances, *J. Spacecr. Rockets*, **22**, 385–393 (1985)
3. Mahaney, J. and Thornton, E. A. Self-shadowing effects on the thermal–structural response of orbiting trusses, *J. Spacecr. Rockets*, **24**, 342–348 (1987)
4 Ko, W. L. Solution accuracies of finite element reentry heat transfer and thermal stress analyses of space shuttle orbiter, *Int. J. Num. Meth. Eng.*, **25**, 517–543 (1988)
5 Givoli, D. and Rand, O. Thermoelastic analysis of space structures in periodic motion, *J. Spacecr. Rockets*, **28**, 457–464 (1991)
6 Rand, O. and Givoli, D. An integrated thermoelastic–analysis for periodically loaded space structures, *Proc. 17th Congr. ICAS, Stockholm*, pp. 1529–1533 (1990)
7 Brogren, E. W., Barclay, D. L. and Straayer, J. W. Simplified thermal estimation techniques for large space structures, *NASA-CR-145253* (1977)
8 Mahaney, J., Thornton, E. A. and Dechaumphai, P. Integrated thermal–structural analysis of large space structures, in *Computational Aspects of Heat Transfer in Structures Symposium*, NASA Langley Research Center, Hampton, *NASA CP-2216*, pp. 179–198 (1981)
9 Lutz, J. D., Allen, D. H. and Haisler, W. E. Finite-element model for the thermoelastic analysis of large composite space structures, *J. Spacecr. Rockets*, **24**, 430–436 (1987)
10 Chin, J. H., Frank, D. R. and Winget, J. M. Engineering finite element analysis of large three-dimensional heat transfer problems, in *Numerical Methods in Thermal Problems* (Eds. R. W. Lewis and K. Morgan), Pineridge Press, Swansea, pp. 341–352 (1985)
11 Rand, O. and Givoli, D. A finite element spectral method with application to the thermoelastic analysis of space structures, *Int. J. Num. Meth. Eng.* **30**, 291–306 (1990)
12 Hughes, T. J. R. *The Finite Element Method*, Prentice Hall, Englewood Cliffs, NJ (1987)
13 Lewandowski, R. Nonlinear steady state vibration of structures by harmonic balance/finite element method, *Proc. 2nd World Congr Comput. Mech.*, Stuttgart (1990)
14 Rand, O. Harmonic variables—a new approach to nonlinear periodic problems, *J. Comp. Math. Appl.*, **15** 953–961 (1988)